

Cooperative UAVs Placement Optimization for Best Multistatic Time-of-Arrival Localization in 5G Networks

Yuan Zhang^{ID}, *Graduate Student Member, IEEE*, Rui Wang^{ID}, *Senior Member, IEEE*, and Erwu Liu^{ID}, *Senior Member, IEEE*

Abstract—The fifth generation (5G) positioning, a breakthrough in cellular navigation, revolutionizes location services. Multistatic time-of-arrival (TOA) 5G localization is a topic of significant interest due to its exceptional performance benefits. The spatial arrangement of unmanned aerial vehicles (UAVs) and the positions of the targets play a crucial role in precisely determining the target's location in 5G environments. This study introduces a novel approach to enhance multistatic 5G localization performance through the placement optimization of UAVs. The derivation of the Cramér-Rao lower bound (CRLB) for TOA-based multistatic 5G localization is given, using unit norm vectors instead of conventional trigonometric parameterizations. A distinctive dual iteration majorization-minimization (DIMM) algorithm is derived, grounded in the MM principle. Our method outperforms current state-of-the-art algorithms tailored for uncorrelated noise in measurements, as it effectively addresses both uncorrelated and correlated noise scenarios. Additionally, the proposed method outperforms both gradient descent and alternating directions method of multipliers (ADMM) approaches in terms of performance. A comprehensive analysis of computational complexity and convergence attests to the pragmatic viability of our methodology. Rigorous simulations affirm its effectiveness across diverse noise variances and UAV-target distances.

Index Terms—Multistatic localization, 5G, D-optimal criteria, optimal UAV placement, Cramér-Rao lower bound (CRLB), majorization-minimization.

I. INTRODUCTION

THE fifth generation (5G) [1], [2] (also known as new radio (NR)) positioning, a breakthrough in cellular navigation, revolutionizes location services. On one hand, as 5G communication systems transition to higher frequency bands, these systems gain access to significantly wider system bandwidths. The frequency range 2 (FR2), as defined by the 3rd

Received 30 June 2024; revised 3 December 2024; accepted 12 January 2025. Date of publication 29 January 2025; date of current version 11 April 2025. This work was supported in part by the National Natural Science Foundation of China under Grant 62271352 and in part by the National Science Foundation of Shanghai under Grant 22ZR1465100. The associate editor coordinating the review of this article and approving it for publication was W. Ni. (*Corresponding author: Rui Wang*)

Yuan Zhang was with the College of Electronics and Information Engineering, Tongji University, Shanghai 201804, China. He is now with the School of Mechanical and Automotive Engineering, Anhui University of Engineering, Wuhu 241000, China (e-mail: yuanzhang@ahpu.edu.cn).

Rui Wang is with the College of Electronics and Information Engineering and Shanghai Institute of Intelligent Science and Technology, Tongji University, Shanghai 201804, China (e-mail: ruiwang@tongji.edu.cn).

Erwu Liu is with the College of Electronics and Information Engineering, Tongji University, Shanghai 201804, China (e-mail: erwuli@tongji.edu.cn). Digital Object Identifier 10.1109/TWC.2025.3532411

Generation Partnership Project (3GPP) for 5G New Radio (NR), encompasses millimeter wave (mmWave) frequencies in the high-frequency spectrum and allows for a maximum system bandwidth significantly larger than previous generations. This wider bandwidth enhances the precision of localization, resulting in higher accuracy for 5G positioning systems. On the other hand, multistatic localization utilizes a single transmitter to emit signals toward the target object, while a distributed array of spatially separated receivers captures the reflected signals. Compared to circular-TOA localization, multistatic localization can be further categorized into two approaches: multistatic-TOA localization and multistatic-TDOA localization, each offering distinct methodologies for position estimation based on time measurements. Besides, multistatic unmanned aerial vehicle (UAV) configurations [3], [4], [5] can be used to achieve higher accuracy in localization and tracking. Multistatic UAV configurations allow signals to be received from multiple directions, which helps improve the accuracy of localization and can overcome challenges such as signal obstruction and multipath propagation [6]. Optimal UAV placement is a critical topic that has significant implications across a myriad of domains, ranging from source localization [7], [8] and tracking [9], [10] to cellular navigation [11]. The crux of optimal UAV placement lies in strategically positioning UAVs within predefined constraints to optimize a chosen performance metric, such as the determinant or trace. In the realms of source localization and tracking, the key goal is to maximize the estimator information matrix of the UAV or target state [12], [13], [14]. Similarly, navigation applications emphasize the optimal placement of UAVs, like mobile receivers, observing known sources, aiming to maximize the estimator information matrix of the UAV's estimation state [15], [16].

While time-of-arrival (TOA) 5G localization methods are widely adopted, the emerging multistatic-TOA-based localization methods offer a distinct set of advantages. In contrast to TOA-based localization, multistatic-TOA-based localization [17], [18] obviates the need for cooperation between the object and UAVs, as well as the requirement for time synchronization between them, streamlining implementation. Furthermore, extensive empirical evidence indicates that multistatic-TOA-based localization yields heightened localization accuracy compared to time difference of arrival (TDOA)-based localization, particularly in scenarios where all UAVs are time synchronized [19]. Moreover, the versatility of

multistatic localization is highlighted by its applicability in scenarios where some or all UAVs possess time synchronization, making it adaptable to a wide range of practical settings.

In previous research, optimal UAV configuration problems for TOA-based localization have often been addressed by formulating them as optimal motion control and uncertainty optimization problems [18], [20]. The former method is frequently used to optimize the UAV path, with the aim of reducing estimation uncertainties, as seen in references like [21]. Decisions regarding UAV path design can be determined through one-step or multi-step lookahead optimizations. These optimization challenges typically involve various nonlinear constraints, arising from physical and geometric factors like maintaining a safe distance from targets, ensuring communication range between UAVs, and avoiding obstacles and threats. However, such optimal control problems generally lack closed-form solutions and require numerical techniques such as gradient-descent methods [18], parameterized unconstrained optimization [21], and differential inclusion solutions [22] for resolution.

For this reason, we present a novel dual iteration majorization-minimization (DIMM) approach for optimal UAV placement in multistatic-TOA-based 5G localization. This approach stands in alignment with the design of experiments theory [23], invoking optimality criteria like *D-optimality*, pivotal in determining the optimal UAV-target geometry. Strikingly, our approach bridges a critical gap in existing literature by conducting a comprehensive exploration of optimal UAV placement strategies specifically tailored to localization based on multistatic TOA in a two-dimensional (2D) plane. Within this framework, a stationary transmitter coexists with multiple receivers, holding potential for incorporating mobile receivers. By orchestrating the optimization of UAV placement within this unique context, we unlock the full potential of multistatic-TOA-based localization, augmenting the domain of wireless communication systems. Our work transcends the realm of theoretical advancements, extending practical implications for real-world applications featuring multistatic geometry UAV-target configurations.

However, current limitations in the field must be acknowledged. Most existing research has predominantly focused on uncorrelated measurement noise scenarios. The research community has yet to comprehensively explore and utilize optimal UAV placement strategies in this specific context. This gap highlights the need for our novel dual iteration majorization-minimization approach, which not only addresses this gap but also redefines the landscape of optimal UAV placement for multistatic TOA-based localization. In fact, the majority of analytical approaches to the multistatic TOA model generally assume the measurements' noise to be independent. However, this assumption proves overly restrictive, particularly in contexts such as urban environments and scenarios affected by multipath effects. In these settings, the noise in UAV TOA measurements often exhibits correlations, and in practical applications, the variance of this noise is typically unequal across measurements. Consequently, there arises a critical need to develop methodologies capable of efficiently designing optimal sensor configurations for multistatic TOA localiza-

tion models, accommodating both correlated and uncorrelated noise scenarios.

In this paper, we present a novel DIMM technique within the context of optimal UAV placement, specifically focusing on multistatic-TOA-based 5G localization, addressing both correlated and uncorrelated noise scenarios. The nonconvex design problem is initially redefined through the Fenchel formulation, thereby converting it into an equivalent saddle-point problem. This problem is subsequently addressed using the MM algorithm, which effectively updates both primal and dual variables. The proposed DIMM approach serves to overcome existing constraints, contributing to an improved grasp of optimizing UAV-target geometry.

The salient points of our contributions are as follows:

- **Optimization Method:** We proceed to formulate our design objectives for multistatic localization by embracing D-optimal criteria grounded in the CRLB. For multistatic 5G localization, we derive a novel DIMM algorithm underpinned by the MM principle. Our DIMM technique distinguishes itself from conventional methods, which exclusively manipulate primal optimization variables. Our method possesses a significant advantage over the prevailing state-of-the-art algorithms, primarily characterized by their analytical nature. Unlike these methods, which are predominantly designed for handling uncorrelated noise in measurements, our approach excels in accommodating both uncorrelated and correlated noise scenarios.
- **Analysis of Computational Complexity and Convergence:** A thorough analysis of computational complexities and convergence is undertaken to underscore the feasibility and effectiveness of our proposed algorithm. This detailed examination not only highlights the practical viability of our approach but also provides valuable insights into its potential applications across various contexts.
- **Numerical Simulations:** We substantiate the viability and robustness of our methodology through extensive numerical simulations. Additionally, the proposed method outperforms both gradient descent and alternating directions method of multipliers (ADMM) approaches in terms of performance. By subjecting our approach to varying noise variances and diverse UAVs-target distances, we empirically demonstrate its effectiveness in designing optimal UAV placements for multistatic localization scenarios.

The paper's structure is outlined as follows: In Section II, the problem formulation is introduced. Section III gives a more direct proof and review in multistatic localization. Section IV delves into the derivation of the proposed DIMM algorithm. The simulations are elaborated upon in Section V. Finally, Section VI encapsulates the conclusion.

Notations: Vectors, matrices, and their notations are vital in this context. They are denoted by bold lowercase letters (e.g., \mathbf{b}) and bold uppercase letters (e.g., \mathbf{C}). The i th element of vector \mathbf{b} is represented as b_i . For the matrix \mathbf{C} , its i th column

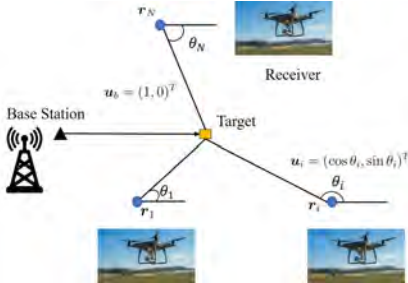


Fig. 1. TOA-based multistatic localization scenario.

is denoted as c_i . The Euclidean norm for a vector \mathbf{b} is indicated as $\|\mathbf{b}\|$. The notations $\text{Tr}(\mathbf{C})$, $\lambda_{\max}(\mathbf{C})$, and $\det(\mathbf{C})$, represent the trace, maximum eigenvalue, and determinant of a matrix, respectively. The diagonal matrix is denoted as $\text{diag}(\mathbf{a})$. The natural logarithm is represented as $\log(\cdot)$, and the identity matrix of size $m \times m$ is denoted as \mathbf{I}_m .

II. PROBLEM FORMULATION

The assessment of error statistics is conducted in the presence of multipath conditions. The channel impulse response (CIR) is simulated using ray-tracing, as described in [24]. The orthogonal frequency division multiplexing (OFDM) symbol is transmitted in a multipath fading channel, which is assumed to stay constant over the duration of a symbol and has the CIR as [25]

$$h(\tau) = \sum_{l=0}^{L-1} \alpha_l \delta(\tau - \tau_l), \quad (1)$$

where L representing the count of multipath components, α_l and τ_l denote the relative attenuation and delay components of the l th path concerning the first path. Furthermore, multipath fading in TOA estimation can cause errors in the estimated distance between the base station and receiver. This issue arises due to multipath propagation, wherein delayed signal components resulting from reflections, diffractions, or scattering interfere with the direct path signal. In scenarios where a multipath component exhibits greater strength than the direct signal, the receiver may incorrectly identify it as the direct path. This misidentification leads to inaccuracies in TOA measurements, thereby degrading positioning accuracy [26].

In the 2D plane, we have a scenario involving multistatic TOA with one transmitter and N available UAVs for positioning a source. This is illustrated in Fig. 1. The unknown position of the target is denoted by $\mathbf{p} = [x, y]^T$, while $\mathbf{r}^t = [x^t, y^t]^T$ represents the transmitter's position. Additionally, $\mathbf{r}_i = [x_i, y_i]^T$, where $1 \leq i \leq N$, corresponds to the position of the i th UAV. In Fig. 1, the reference frame is adaptable to arbitrary rotations, enabling us to assume the unit vector $\mathbf{u}_b = [1, 0]^T$, corresponding to a transmitter bearing angle of $\theta_b = 0$ radians. \mathbf{u}_i is the unit vector pointing from the transmitter to the i th UAV.

The TOA measurement between the i th UAV and the target can be expressed as

$$\hat{\tau}_i = \tau_i(\mathbf{p}) + e_i, \quad (2)$$

$$\tau_i(\mathbf{p}) = \frac{\|\mathbf{p} - \mathbf{r}^t\| + \|\mathbf{p} - \mathbf{r}_i\|}{c}, \quad (3)$$

where c is the propagation speed, and the measurement error, denoted as e_i , is represented as zero-mean independent Gaussian white noise with a variance of σ_i^2 . These variances are assumed to be constant and predetermined for the optimal UAV placement.

By multiplying both sides of equation (2) by c , we can rewrite the TOA range measurement in a vector form gives

$$\hat{\mathbf{d}} = \mathbf{d}(\mathbf{p}) + \mathbf{v}, \quad (4)$$

where $\mathbf{d} = [d_1, d_2, \dots, d_N]^T$ and $\mathbf{v} = [v_1, v_2, \dots, v_N]^T$. The covariance matrix of TOA measurements is denoted by $\mathbf{R} = \mathbb{E}[\mathbf{v}\mathbf{v}^T]$, and this covariance matrix is

$$\mathbf{R} = \mathbb{E}[\mathbf{v}\mathbf{v}^T] = \text{diag}(\sigma_1^2, \dots, \sigma_N^2) \quad (5)$$

with $\sigma_i^2 = c^2 \sigma_i^2$. To solve equation (4) for \mathbf{p} , at least two receivers ($N \geq 2$) are necessary, since there are two unknown variables, x and y . However, to guarantee a unique solution, a minimum of three receivers ($N \geq 3$) is required. This is because with only two receivers, the resulting TOA measurements form two ellipses that may intersect at two different points, leading to ambiguity in the target's position. Nonetheless, if some prior information about the target's approximate location is available, two receivers ($N = 2$) could still be sufficient to resolve this ambiguity and accurately localize the target.

In the context of 5G systems, concerning the OFDM signal, the variance¹ of v_i can be calculated by

$$\sigma_i^2 = \text{var}(v_i) = \frac{c^2 T_s^2}{8\pi^2 \text{SNR}_i \sum_{n \in \mathcal{N}_{\text{PRS}}} p_n^2 n^2}, \quad (6)$$

where T_s represents the OFDM symbol duration, \mathcal{N}_{PRS} refers to the subset of subcarriers dedicated to the positioning reference signal (PRS), while p_n^2 signifies the relative power weight assigned to the n th subcarrier. SNR_i denotes signal noise ratio (SNR) at the i th BS. Multistatic positioning entails a transmitter emitting a signal. The emitted signal undergoes reflection or relay by the object under localization, after which it is received by a UAV. An ellipsoidal surface is subsequently generated, illustrating potential object locations determined by signal propagation time from the transmitter to the UAV passing through the object. The positions of the transmitter and UAV serve as the foci of this ellipsoid.

For the Gaussian function in the context of TOA multistatic measurements, the conditional probability density function of \mathbf{d} is expressed as:

$$f(\mathbf{d}|\mathbf{p}) = \frac{1}{\sqrt{(2\pi)^N \det(\mathbf{R})}} \times \exp \left\{ -\frac{1}{2} (\hat{\mathbf{d}} - \mathbf{d}(\mathbf{p}))^\top \mathbf{R}^{-1} (\hat{\mathbf{d}} - \mathbf{d}(\mathbf{p})) \right\}. \quad (7)$$

In order to achieve highly accurate estimation of the source location, we strive to optimize the UAV geometry. The precision of this estimation can be quantified by determining the minimum possible estimation error, which can be obtained

¹According to [27], (6) is obtained from the Cramér-Rao lower bound (CRLB) of the time delay estimation. In [27], the CRLB of the TOA estimation was derived rigorously by directly using discrete Fourier transform.

from the CRLB matrix. The CRLB matrix is derived from the inverse of the FIM. Specifically, when estimating \mathbf{p} from the measurement vector \mathbf{d} , the FIM is given by the following expression:

$$\mathbf{M} = \mathbb{E} \left\{ \left(\frac{\partial}{\partial \mathbf{p}} \ln f(\mathbf{d} | \mathbf{p}) \right) \left(\frac{\partial}{\partial \mathbf{p}} \ln f(\mathbf{d} | \mathbf{p}) \right)^T \right\}. \quad (8)$$

The partial derivative of the logarithm of the conditional probability density function $\ln f(\mathbf{d} | \mathbf{p})$ with respect to \mathbf{p} is given by

$$\frac{\partial}{\partial \mathbf{p}} \ln f(\mathbf{d} | \mathbf{p}) = -\frac{\partial \mathbf{d}^T}{\partial \mathbf{p}} \mathbf{R}^{-1} (\hat{\mathbf{d}} - \mathbf{d}) = -\mathbf{H}^T \mathbf{R}^{-1} (\hat{\mathbf{d}} - \mathbf{d}), \quad (9)$$

where \mathbf{H} is the Jacobian matrix of $\mathbf{d}(\mathbf{p})$ in (4) with respect to the true value \mathbf{p} :

$$\mathbf{H} = [\mathbf{g}_1, \dots, \mathbf{g}_N]^T = [\mathbf{u}_b + \mathbf{u}_1, \dots, \mathbf{u}_b + \mathbf{u}_N]^T. \quad (10)$$

Here we define \mathbf{u}_i as the unit vector pointing from the emitter to the UAVs as shown in Fig. 1. It can be expressed as

$$\mathbf{u}_i = [\cos \theta_i, \sin \theta_i]^T = \begin{bmatrix} \frac{x-x_i}{\sqrt{(x-y_i)^2 + (y-y_i)^2}} \\ \frac{y-y_i}{\sqrt{(x-y_i)^2 + (y-y_i)^2}} \end{bmatrix}, \quad (11)$$

where θ_i is the bearing angle of i th receiver. Inserting (9) into (8) gives the FIM as

$$\begin{aligned} \mathbf{M} &= \mathbb{E}\{\mathbf{H}^T \mathbf{R}^{-1} (\hat{\mathbf{d}} - \mathbf{d})(\hat{\mathbf{d}} - \mathbf{d})^T \mathbf{R}^{-1} \mathbf{H}\} \\ &= \mathbf{H}^T \mathbf{R}^{-1} \mathbb{E}\{(\hat{\mathbf{d}} - \mathbf{d})(\hat{\mathbf{d}} - \mathbf{d})^T\} \mathbf{R}^{-1} \mathbf{H} \\ &= \mathbf{H}^T \mathbf{R}^{-1} \mathbf{H}. \end{aligned} \quad (12)$$

The α -confidence error ellipsoid can be defined as the minimum volume ellipsoid containing $\mathbf{p} - \hat{\mathbf{p}}$ with a probability of α . This ellipsoid is represented as:

$$E_\alpha = \left\{ \mathbf{p} \mid (\mathbf{p} - \hat{\mathbf{p}})^T \Sigma_{\hat{\mathbf{p}}}^{-1} (\mathbf{p} - \hat{\mathbf{p}}) \leq c_{\text{cov}} \right\}, \quad (13)$$

where $c_{\text{cov}} = F_{\chi_n^2}^{-1}$, $\Sigma_{\hat{\mathbf{p}}}$ denotes a theoretical error covariance. The cumulative distribution function $F_{\chi_n^2}$ can be described as the probability distribution function that represents the cumulative probability of obtaining a value less than or equal to a specified value from a chi-squared distribution with ' n ' degrees of freedom.

In D-optimal design, the goal is to reduce the volume of the α -confidence error ellipsoid:

$$\text{volume}(E_\alpha) = \frac{(c_{\text{cov}}\pi)^{n/2}}{\Gamma((n/2) + 1)} \det(\mathbf{H}^T \mathbf{R}^{-1} \mathbf{H})^{-1/2}, \quad (14)$$

where Γ is Gamma function.

Note that if we directly minimize the function in (14), the solution may be numerically unstable and reduce computational efficiency. To this end, we have

$$\begin{aligned} \log \text{volume}(E_\alpha) &= \frac{n}{2} \log(c_{\text{cov}}\pi) - \log \left(\Gamma \left(\frac{n}{2} + 1 \right) \right) \\ &\quad - \frac{1}{2} \log \det(\mathbf{H}^T \mathbf{R}^{-1} \mathbf{H}). \end{aligned} \quad (15)$$

In (15), the first two terms are constants reliant solely on c and n . Solving (15) presents challenges due to the quadratic term within $\log \det(\cdot)$. In the following, we introduce an MM-based method to tackle the complex nonlinear optimization issue.

When considering the D-optimality criterion, the challenge of optimal UAV placement for multistatic localization can be defined as the subsequent optimization problem:

$$\begin{aligned} \max_{\mathbf{U} \in \Phi} \log \det(\mathbf{H}^T \mathbf{R}^{-1} \mathbf{H}) \\ \text{s.t. } \mathbf{H} = \mathbf{U}_b + \mathbf{U}, \end{aligned} \quad (16)$$

where the set Φ satisfies

$$\Phi = \{\mathbf{u} \mid \|\mathbf{u}_i\| = 1; \forall i\}. \quad (17)$$

III. OPTIMAL UAV PLACEMENT IN THE PRESENCE OF UNCORRELATED NOISE MEASUREMENTS

In this section, we first present an optimal geometry analysis for multistatic TOA localization involving one transmitter or base station and multiple UAVs in the presence of uncorrelated noise measurements. In contrast to the prior study by [18], we present a more straightforward proof. This is also meant to compare the analytical conclusion with the DIMM method that we have proposed.

Initially, the Jacobian matrix \mathbf{H} undergoes re-parameterization using the bearing angles $\{\theta_i\}_{i=1}^N$, which represent the angles between the target and the N UAVs, as depicted in Fig. 1. Subsequently, the matrix \mathbf{H} can be re-expressed as $\mathbf{H} = [\mathbf{p} \ \mathbf{q}]$, where $\mathbf{p} \triangleq [1 + \cos \theta_1, \dots, 1 + \cos \theta_N]^T$ and $\mathbf{q} \triangleq [\sin \theta_1, \dots, \sin \theta_N]^T$. The matrix $\mathbf{M} = \mathbf{H}^T \mathbf{R}^{-1} \mathbf{H}$ may be expressed as

$$\mathbf{M} = \mathbf{H}^T \mathbf{R}^{-1} \mathbf{H} = \begin{bmatrix} \mathbf{p}^T \mathbf{R}^{-1} \mathbf{p} & \mathbf{p}^T \mathbf{R}^{-1} \mathbf{q} \\ \mathbf{q}^T \mathbf{R}^{-1} \mathbf{p} & \mathbf{q}^T \mathbf{R}^{-1} \mathbf{q} \end{bmatrix}, \quad (18)$$

which has the determinant

$$\det(\mathbf{M}) = (\mathbf{p}^T \mathbf{R}^{-1} \mathbf{p})(\mathbf{q}^T \mathbf{R}^{-1} \mathbf{q}) - (\mathbf{p}^T \mathbf{R}^{-1} \mathbf{q})(\mathbf{q}^T \mathbf{R}^{-1} \mathbf{p}). \quad (19)$$

Theorem 1: The maximum value of the objective function (19) is equal to

$$\frac{27}{16} \left(\sum_{i=1}^N \frac{1}{\sigma_i^2} \right)^2. \quad (20)$$

and this maximum value is reached when

$$\begin{aligned} \sum_{i=1}^N \frac{p_i^2}{\sigma_i^2} &= \frac{9}{4} \sum_{i=1}^N \frac{1}{\sigma_i^2}, \\ \cos \theta_1 &= \dots = \cos \theta_N \\ &= 1/2, \left(\sum_{i=1}^N \frac{1}{\sigma_i^2} (1 + \cos \theta_i) \sin \theta_i \right)^2 = 0. \end{aligned} \quad (21)$$

Proof: The determinant of \mathbf{M} may be expressed by

$$\det(\mathbf{M}) \leq (\mathbf{p}^T \mathbf{R}^{-1} \mathbf{p})(\mathbf{q}^T \mathbf{R}^{-1} \mathbf{p}), \quad (22)$$

where the equality holds if $(\mathbf{p}^T \mathbf{R}^{-1} \mathbf{q})(\mathbf{q}^T \mathbf{R}^{-1} \mathbf{p}) = 0$. Using the definition of \mathbf{p} and \mathbf{q} , the following can be deduced

$$\begin{aligned} & \mathbf{p}^T \mathbf{R}^{-1} \mathbf{q} + \mathbf{q}^T \mathbf{R}^{-1} \mathbf{p} \\ &= \sum_{i=1}^N \frac{1}{\sigma_i^2} (1 + \cos \theta_i)^2 \\ &+ \sum_{i=1}^N \frac{1}{\sigma_i^2} \sin \theta_i^2 = \sum_{i=1}^N \frac{1}{\sigma_i^2} (2 + 2 \cos \theta_i). \end{aligned} \quad (23)$$

Defining $p_i \triangleq 1 + \cos \theta_i$ with $0 \leq p_i \leq 2$, incorporating the geometric constraint (23) into (19) yields

$$\begin{aligned} \det(\mathbf{M}) &\leq \sum_{i=1}^N \frac{1}{\sigma_i^2} p_i^2 \sum_{i=1}^N \frac{1}{\sigma_i^2} (2p_i - p_i^2) \\ &= \sum_{i=1}^N \frac{p_i^2}{\sigma_i^2} \left(\sum_{i=1}^N \frac{2p_i}{\sigma_i^2} - \sum_{i=1}^N \frac{p_i^2}{\sigma_i^2} \right). \end{aligned} \quad (24)$$

The following Cauchy-Schwarz inequality holds

$$\left(\sum_{i=1}^N \frac{p_i}{\sigma_i^2} \right)^2 \leq \sum_{i=1}^N \frac{1}{\sigma_i^2} \sum_{i=1}^N \frac{p_i^2}{\sigma_i^2}$$

with equality if and only if $p_1 = \dots = p_N$. Noting that p_i satisfies $0 \leq p_i \leq 2$, we have

$$\sum_{i=1}^N \frac{p_i}{\sigma_i^2} \leq \left(\sum_{i=1}^N \frac{1}{\sigma_i^2} \right)^{\frac{1}{2}} \left(\sum_{i=1}^N \frac{p_i^2}{\sigma_i^2} \right)^{\frac{1}{2}}. \quad (25)$$

Defining $m = \sum_{i=1}^N \frac{a_i^2}{\sigma_i^2}$ and $a = \sum_{i=1}^N \frac{1}{\sigma_i^2}$, we have

$$T(m) = 2a^{\frac{1}{2}}m^{\frac{3}{2}} - m^2, \quad (26)$$

$$\det(\mathbf{M}) \leq T(m). \quad (27)$$

In the upcoming discussion, our objective is to maximize the expression on the right-hand side of Equation (27). Computing the first derivative of f with respect to m gives

$$T'(m) = 3a^{\frac{1}{2}}m^{\frac{1}{2}} - 2m = 0. \quad (28)$$

The maximum value of the right-hand side of (27) is reached when the following conditions are met:

$$m = \frac{9a}{4}. \quad (29)$$

Note that the premise of the above derivation is to satisfy the condition $(\mathbf{p}^T \mathbf{R}^{-1} \mathbf{p})(\mathbf{q}^T \mathbf{R}^{-1} \mathbf{p}) = 0$, thus we expand \mathbf{q} and \mathbf{p} to get the following:

$$(\mathbf{p}^T \mathbf{R}^{-1} \mathbf{p})(\mathbf{q}^T \mathbf{R}^{-1} \mathbf{p}) = \left(\sum_{i=1}^N \frac{1}{\sigma_i^2} (1 + \cos \theta_i) \sin \theta_i \right)^2. \quad (30)$$

Therefore, the determinant's maximum value is equivalent to

$$\max(\det(\mathbf{M})) = \frac{27a^2}{16} = \frac{27}{16} \left(\sum_{i=1}^N \frac{1}{\sigma_i^2} \right)^2. \quad (31)$$

and this maximum value is attained when the following conditions are satisfied:

$$\begin{aligned} m &= \sum_{i=1}^N \frac{p_i^2}{\sigma_i^2} = \frac{9}{4} \sum_{i=1}^N \frac{1}{\sigma_i^2}, \\ p_1 &= \dots = p_N, \\ \left(\sum_{i=1}^N \frac{1}{\sigma_i^2} (1 + \cos \theta_i) \sin \theta_i \right)^2 &= 0. \end{aligned}$$

Therefore, maximum value of the determinant is attained when the condition $p_1 = \dots = p_N = 3/2$ is satisfied, i.e., $|\theta_i| = \pi/3, i = 1, \dots, N$ and $\left(\sum_{i=1}^N \frac{1}{\sigma_i^2} (1 + \cos \theta_i) \sin \theta_i \right)^2 = 0$. ■

The analytical proof we propose offers a more straightforward way for the case where N is even, providing a supplement to the analysis in [16]. However, the method introduced here is applicable exclusively to scenarios where N is an even number. The analysis of applicability to both odd and even values of N has been thoroughly addressed in [16], which concludes that the parity of N does not influence the optimal angular configuration $|\theta_i| = \pi/3$ for all $i = 1, \dots, N$, regardless of whether the proof method is simplified. The provided theorem presents a key result for maximizing the optimization problem (19). It states that the maximum value of the objective function is equal to $\frac{27}{16} \left(\sum_{i=1}^N \frac{1}{\sigma_i^2} \right)^2$. Furthermore, the theorem specifies the conditions under which this maximum value is achieved. When these conditions are met, the objective function will achieve its maximum value as stated in the theorem. The result provides valuable insights into the optimization problem and offers a clear mathematical expression for the optimal solution. These results are highly significant as they reveal the optimal configurations of θ_2 and θ_3 that yield maximum values of the FIM determinant for different UAV variance scenarios.

Analytical solutions provide valuable insights into how the UAV-target geometry influences the accuracy of target localization and tracking. It's important to highlight that although these solutions may not directly address optimal path planning, they furnish crucial information for comprehending and enhancing localization and tracking procedures. As a result, problems related to optimal UAV placement are articulated as challenges in optimal control and parameter optimization. In the subsequent section, we explore the formulation of efficient optimal control problems using an optimization approach for optimal UAV placement.

IV. PROPOSED DIMM ALGORITHM FOR MULTISTATIC 5G LOCALIZATION

In the preceding analysis, we derive the optimal UAV configuration for multistatic localization using a CRLB analysis approach. However, this analysis assumes that the measurement noise is independent, whereas in practical applications, the measurement noise may also be correlated. Additionally, the true position of the target is assumed to be known, as derived in (9). Therefore, in this section, we propose an optimization method to further address the UAV configuration problem in the presence of correlated noise.

This section commences by providing a concise introduction to the MM framework, which serves as the fundamental structure underpinning the algorithm introduced in this context. Subsequently, a comprehensive elucidation of the algorithms devised for addressing the multistatic localization problem follows. The section culminates by delving into an examination of the computational complexity, along with a presentation of the proof showcasing the the DIMM algorithm convergence.

A. MM Method

The MM framework leverages the inherent structure of the problem and devises an algorithm tailored to its specific characteristics. This approach unfolds through a two-step process. The initial step involves majorization, wherein a surrogate function is formulated to envelop the objective function on a global scale, while ensuring that the disparity between them is minimized. The subsequent step focuses on minimization in which the surrogate function derived from the preceding phase is systematically reduced to its minimum value.

Let's consider the optimization problem below:

$$\begin{aligned} \min_{\mathbf{x}} \quad & \phi(\mathbf{x}) \\ \text{s.t. } \mathbf{x} \in & \varphi, \end{aligned} \quad (32)$$

where φ represents a non-empty closed set. An initial point $\mathbf{x}_0 \in \varphi$ is chosen, and the MM algorithm generates then a sequence of feasible points \mathbf{x}_t . At the point \mathbf{x}_t , a surrogate function $t(\mathbf{x}|\mathbf{x}_t)$ first is obtained satisfying the following conditions:

$$t(\mathbf{x}|\mathbf{x}_t) \geq \phi(\mathbf{x}), \quad \forall \mathbf{x} \in \varphi, \quad t(\mathbf{x}_t|\mathbf{x}_t) = \phi(\mathbf{x}_t). \quad (33)$$

In the following minimization step, \mathbf{x} undergoes an update given by

$$\mathbf{x}_{t+1} = \arg \min_{\mathbf{x} \in \varphi} t(\mathbf{x}|\mathbf{x}_t). \quad (34)$$

The following inequality is derived from equations (33) and (34) as follows:

$$\phi(\mathbf{x}_{t+1}) \leq t(\mathbf{x}_{t+1}|\mathbf{x}_t) \leq t(\mathbf{x}_t|\mathbf{x}_t) = \phi(\mathbf{x}_t). \quad (35)$$

This process establishes the monotonic decrease of the sequence $(\phi(\mathbf{x}_t))$, signifying that the objective function consistently diminishes under the influence of MM. The effectiveness of the MM technique hinges upon the meticulous design of the surrogate function. A crucial aspect lies in formulating a surrogate function that is not only smooth and convex but also amenable to separation of variables. Such characteristics facilitate efficient and scalable minimization, paving the way for the development of easily implementable algorithms. Nevertheless, a delicate balance exists when constructing a surrogate function, involving the trade-off between achieving rapid convergence and maintaining minimal computational complexity and memory usage per iteration. Striking this equilibrium is pivotal for the successful deployment of the MM approach. The delicate interplay between these elements guarantees that the surrogate function closely mimics the objective function's shape, facilitating rapid convergence. Simultaneously, it retains simplicity in its minimization process to maintain manageable computational demands.

B. The Proposed DIMM Algorithm for Multistatic 5G Localization

In order to address the intricate nature of the objective function presented in equation (32), we introduce an auxiliary variable \mathbf{X} and undertake a reformulation of the original problem (16) through the utilization of the Fenchel conjugate representation [28]. This transformation leads to the emergence of an equivalent saddle-point problem, denoted as follows:

$$\begin{aligned} \max_{\mathbf{U} \in \Phi} \min_{\mathbf{X} \succeq 0} \quad & \text{Tr}(\mathbf{XH}^\top \mathbf{R}^{-1} \mathbf{H}) - \log \det(\mathbf{X}) \\ \text{s.t. } \mathbf{H} = & \mathbf{U}_b + \mathbf{U}, \end{aligned} \quad (36)$$

where variable \mathbf{U} is assumed to be the primal variable, while variable \mathbf{X} is dual variable. We will now develop a method to address the maximin problem presented in (36). Let

$$h(\mathbf{H}) = \min_{\mathbf{X} \succeq 0} \text{Tr}(\mathbf{XH}^\top \mathbf{R}^{-1} \mathbf{H}) - \log \det(\mathbf{X}) \quad (37)$$

be a function only in \mathbf{H} . Then the problem (37) can be rewritten given by:

$$\begin{aligned} \max_{\mathbf{U} \in \Phi} \quad & h(\mathbf{H}) \\ \text{s.t. } \mathbf{H} = & \mathbf{U}_b + \mathbf{U}. \end{aligned} \quad (38)$$

We can employ the MM method to iteratively maximize the lowerbound of $h(\mathbf{H})$. This is achieved by first considering the first term of $h(\mathbf{H})$ in (37), i.e., $\text{Tr}(\mathbf{XH}^\top \mathbf{R}^{-1} \mathbf{H})$, which is a convex function in \mathbf{H} for any \mathbf{X} . As (38) is a maximization problem, the order of operations is altered to maximize the lowerbound. Therefore, we can make an upperbound operation for the convex term at any $\mathbf{H} = \mathbf{H}_l$ by using first-order Taylor's expansion

$$\begin{aligned} \text{Tr}(\mathbf{XH}^\top \mathbf{R}^{-1} \mathbf{H}) \geq 2\text{Tr}(\mathbf{XH}_l^\top \mathbf{R}^{-1} \mathbf{H}) \\ - \text{Tr}(\mathbf{XH}_l^\top \mathbf{R}^{-1} \mathbf{H}_l), \end{aligned} \quad (39)$$

with the equality if and only if $\mathbf{H} = \mathbf{H}_l$. Given (39), the function $h(\mathbf{H})$ over the variable \mathbf{H} can be upperbounded as

$$\begin{aligned} h(\mathbf{H}) \geq \min_{\mathbf{X} \succeq 0} 2\text{Tr}(\mathbf{XH}_l^\top \mathbf{R}^{-1} \mathbf{H}) \\ - \text{Tr}(\mathbf{XH}_l^\top \mathbf{R}^{-1} \mathbf{H}_l) - \log \det(\mathbf{X}). \end{aligned} \quad (40)$$

Therefore, we have the following surrogate optimization problem:

$$\begin{aligned} \max_{\mathbf{U} \in \Phi} \min_{\mathbf{X} \succeq 0} \quad & 2\text{Tr}(\mathbf{XH}_l^\top \mathbf{R}^{-1} \mathbf{H}) - \text{Tr}(\mathbf{XH}_l^\top \mathbf{R}^{-1} \mathbf{H}_l) \\ & - \log \det(\mathbf{X}) \\ \text{s.t. } \mathbf{H} = & \mathbf{U}_b + \mathbf{U}. \end{aligned} \quad (41)$$

To proceed further, we obtain:

$$\begin{aligned} \max_{\mathbf{U} \in \Phi} \min_{\mathbf{X} \succeq 0} \quad & 2\text{Tr}(\mathbf{X}(\mathbf{U}_b + \mathbf{U}_l)^\top \mathbf{R}^{-1} (\mathbf{U}_b + \mathbf{U})) \\ & - \text{Tr}(\mathbf{X}(\mathbf{U}_b + \mathbf{U}_l)^\top \mathbf{R}^{-1} (\mathbf{U}_b + \mathbf{U}_l)) - \log \det(\mathbf{X}). \end{aligned} \quad (42)$$

The constraint set Φ governing the variable \mathbf{U} can be effectively relaxed to $\tilde{\Phi}$, i.e. $\tilde{\Phi} = \{\mathbf{u} \mid \|\mathbf{u}_i\| \leq 1; \forall i\}$. Optimally, the

relaxation will consistently be tight since the maximum value over \mathbf{U} is achieved solely on the boundary. Consequently, the maximin problem in (42) can be converted as a minimax problem by applying the minimax theorem [28], as succinctly presented in the following lemma:

Lemma 1: Let $\mathcal{X} \in \mathbb{R}^n$ and $\mathcal{Y} \in \mathbb{R}^m$ be compact convex sets. If $f : \mathcal{X} \times \mathcal{Y} \rightarrow \mathbb{R}$ is a continuous concave-convex function, meaning $f(., y) : \mathcal{X} \rightarrow \mathbb{R}$ is concave for given y , and $f(x, .) : \mathcal{Y} \rightarrow \mathbb{R}$ is convex for given x , then:

$$\max_{x \in \mathcal{X}} \min_{y \in \mathcal{Y}} f(x, y) = \min_{y \in \mathcal{Y}} \max_{x \in \mathcal{X}} f(x, y). \quad (43)$$

(42) is a continuous function, which is concave in \mathbf{U} (linear expression) for given \mathbf{X} and convex in \mathbf{X} for given \mathbf{U} . The above relaxation is undertaken with the specific objective of constructing constraint sets (following the relaxation) that are both compact and convex in nature. Therefore Lemma 3.1 can be utilized for the problem in (42). Thus, we have

$$\begin{aligned} & \min_{\mathbf{X} \succeq 0} \max_{\mathbf{U} \in \tilde{\Phi}} 2\text{Tr} \left(\mathbf{X} (\mathbf{U}_b + \mathbf{U}_l)^T \mathbf{R}^{-1} (\mathbf{U}_b + \mathbf{U}) \right) \\ & - \text{Tr} \left(\mathbf{X} (\mathbf{U}_b + \mathbf{U}_l)^T \mathbf{R}^{-1} (\mathbf{U}_b + \mathbf{U}_l) \right) - \log \det(\mathbf{X}). \end{aligned} \quad (44)$$

It is evident that the aforementioned issue entails an inner maximization problem concerning variable \mathbf{U} , coupled with an outer minimization problem revolving around variable \mathbf{X} . Upon resolving the inner minimization dilemma and subsequently substituting the optimal minimizer \mathbf{U}^{opt} , the outcome yields a maximization quandary solely concerning the primal variable \mathbf{U} . Within this context, the objective function (pertaining to \mathbf{X}) serves as a surrogate derived from the MM framework for the original objective articulated in (16). The maximization problem can be expressed as

$$\max_{\mathbf{U} \in \tilde{\Phi}} 2\text{Tr} \left(\mathbf{X} (\mathbf{U}_b + \mathbf{U}_l)^T \mathbf{R}^{-1} \mathbf{U} \right). \quad (45)$$

To proceed further, we obtain

$$\max_{\mathbf{U} \in \tilde{\Phi}} 2\text{Tr} \left(\mathbf{U} \mathbf{X} (\mathbf{U}_b + \mathbf{U}_l)^T \mathbf{R}^{-1} \right). \quad (46)$$

Let $\mathbf{A} = \mathbf{X} (\mathbf{U}_b + \mathbf{U}_l)^T \mathbf{R}^{-1}$, then the problem is rewritten as

$$\max_{\mathbf{U} \in \tilde{\Phi}} 2 \sum_{i=1}^N \mathbf{u}_i^\top \mathbf{a}_i. \quad (47)$$

where \mathbf{a}_i represents the i th column of the matrix \mathbf{A} . Therefore, problem (47) has the following closed-form solution given by

$$\mathbf{u}_i^{\text{opt}} = \frac{\mathbf{a}_i}{\|\mathbf{a}_i\|}. \quad (48)$$

While the solution to the problem is relaxed, it is crucial to emphasize that the relaxed solution maintains a unit norm, and thus, there is no loss in performance.

The original minimization problem (44) is transformed into the following simplified minimization problem given by

$$\min_{\mathbf{X} \succeq 0} \text{Tr} \left(\mathbf{A} \mathbf{U}_b + \mathbf{A} (2\mathbf{U}^{\text{opt}} - \mathbf{U}_l) \right) - \log \det(\mathbf{X}) \quad (49)$$

with $\mathbf{A} = \mathbf{X} \tilde{\mathbf{B}}$ and $\tilde{\mathbf{B}} = (\mathbf{U}_b + \mathbf{U}_l)^T \mathbf{R}^{-1}$. By substituting back $\mathbf{u}_i^{\text{opt}}$ in (49) we get

$$\min_{\mathbf{X} \succeq 0} 2 \sum_{i=1}^N \|\mathbf{a}_i\| + \text{Tr} \left(\mathbf{A} (\mathbf{U}_b - \mathbf{U}_l) \right) - \log \det(\mathbf{X}). \quad (50)$$

Substituting for $\mathbf{a}_i = \mathbf{X} \tilde{\mathbf{b}}_i$ into (50), where \mathbf{b}_i represents the i th column of the matrix \mathbf{B} , we get

$$\begin{aligned} & \min_{\mathbf{X} \succeq 0} 2 \sum_{i=1}^N \|\mathbf{X} \tilde{\mathbf{b}}_i\| + \text{Tr} \left(\mathbf{X} (\mathbf{U}_b + \mathbf{U}_l)^T \mathbf{R} (\mathbf{U}_b - \mathbf{U}_l) \right) \\ & - \log \det(\mathbf{X}). \end{aligned} \quad (51)$$

The problem mentioned can be classified as a convex minimization issue. This problem can be directly addressed using interior point solvers, such as CVX. Nonetheless, using CVX might introduce computational inefficiencies. As an alternative approach, we revisit the use of the MM technique to develop a DIMM algorithm. This method is employed to determine the global minimizer for the problem outlined in (51). The approach includes creating a specialized surrogate function for (51) with a given \mathbf{X}_t . Subsequently, an iterative process is employed to minimize this surrogate, ultimately leading to the optimal solution for the problem as defined in (51).

Given that (51) represents a minimization problem and the inequality [28] $\|\mathbf{X} \tilde{\mathbf{b}}_i\| \leq 1/2 (\|\mathbf{X}_t \tilde{\mathbf{b}}_i\| + \|\mathbf{X} \tilde{\mathbf{b}}_i\|^2 / \|\mathbf{X}_t \tilde{\mathbf{b}}_i\|)$ holds, our initial objective involves establishing an upper bound for the term $\|\mathbf{X} \tilde{\mathbf{b}}_i\|$. This can be expressed as follows:

$$\begin{aligned} g(\mathbf{X}) \leq & \min_{\mathbf{X} \succeq 0} \sum_{i=1}^N \left(\|\mathbf{X}_t \tilde{\mathbf{b}}_i\| + \|\mathbf{X} \tilde{\mathbf{b}}_i\|^2 / \|\mathbf{X}_t \tilde{\mathbf{b}}_i\| \right) \\ & + \text{Tr} \left(\mathbf{X} (\mathbf{U}_b + \mathbf{U}_l)^T \mathbf{R} (\mathbf{U}_b - \mathbf{U}_l) \right) - \log \det(\mathbf{X}). \end{aligned} \quad (52)$$

To proceed further, we get

$$\begin{aligned} g(\mathbf{X}) \leq & \min_{\mathbf{X} \succeq 0} \sum_{i=1}^N \left(\|\mathbf{X}_t \tilde{\mathbf{b}}_i\| + \tilde{\mathbf{b}}_i^\top \mathbf{X}^\top \mathbf{X} \tilde{\mathbf{b}}_i / \|\mathbf{X}_t \tilde{\mathbf{b}}_i\| \right) \\ & + \text{Tr} \left(\mathbf{X} (\mathbf{U}_b + \mathbf{U}_l)^T \mathbf{R}^{-1} (\mathbf{U}_b - \mathbf{U}_l) \right) - \log \det(\mathbf{X}) \\ \triangleq & \tilde{f}(\mathbf{X} | \mathbf{X}_t). \end{aligned} \quad (53)$$

Using $\mathbf{C} = \sum_{i=1}^N \tilde{\mathbf{b}}_i \tilde{\mathbf{b}}_i^\top / \|\mathbf{X}_t \tilde{\mathbf{b}}_i\|$, (53) can be rewritten as

$$\begin{aligned} & \min_{\mathbf{X} \succeq 0} \sum_{i=1}^N \|\mathbf{X}_t \tilde{\mathbf{b}}_i\| + \text{Tr} \left(\mathbf{X} \mathbf{C} \mathbf{X}^\top \right) \\ & + \text{Tr} \left(\mathbf{X} (\mathbf{U}_b + \mathbf{U}_l)^T \mathbf{R}^{-1} (\mathbf{U}_b - \mathbf{U}_l) \right) - \log \det(\mathbf{X}). \end{aligned} \quad (54)$$

The problem defined in (54) lacks a closed-form solution. To this end, we opt to once more establish an upper bound for $\tilde{f}(\mathbf{X} | \mathbf{X}_t)$ at the point $\mathbf{X} = \mathbf{X}_t$. To achieve this, let's denote

$\lambda_1 = \lambda_{\max}(\mathbf{C})$ and introduce a new matrix $\tilde{\mathbf{C}} = \mathbf{C} - \lambda_1 \mathbf{I}$. With these considerations, (54) can be restated as:

$$\begin{aligned} \min_{\mathbf{X} \succeq 0} & \sum_{i=1}^N \|\mathbf{X}_t \tilde{\mathbf{b}}_i\| + \text{Tr}(\mathbf{X} \tilde{\mathbf{C}} \mathbf{X}^\top) + \lambda_1 \text{Tr}(\mathbf{X}^\top \mathbf{X}) \\ & + \text{Tr}(\mathbf{X} (\mathbf{U}_b + \mathbf{U}_l)^\top \mathbf{R}^{-1} (\mathbf{U}_b - \mathbf{U}_l)) - \log \det(\mathbf{X}). \end{aligned} \quad (55)$$

The following *Lemma* will show the concavity of the term $\text{Tr}(\mathbf{X} \tilde{\mathbf{C}} \mathbf{X}^\top)$.

Lemma 2: The term $\text{Tr}(\mathbf{X} \tilde{\mathbf{C}} \mathbf{X}^\top)$ is concave with respect to the matrix variable \mathbf{X} .

Proof: We consider the eigenvalue equation $\tilde{\mathbf{C}}\mathbf{v} = \lambda\mathbf{v}$, where \mathbf{v} represents the eigenvector and λ corresponds to the eigenvalue. Upon substituting $\tilde{\mathbf{C}} = \mathbf{C} - \lambda_1 \mathbf{I}$ into the equation $\tilde{\mathbf{C}}\mathbf{v} = \lambda\mathbf{v}$, we arrive at $(\mathbf{C} - \lambda_1 \mathbf{I})\mathbf{v} = \lambda\mathbf{v}$. By further simplifying, we deduce $\mathbf{C}\mathbf{v} = (\lambda + \lambda_1)\mathbf{v}$. This implies that the condition $(\lambda + \lambda_1) \leq \lambda_1$ holds true. Consequently, we establish that $\lambda \leq 0$. The matrix $\tilde{\mathbf{C}} = \mathbf{C} - \lambda_1 \mathbf{I}$ assumes a negative semi-definite nature, thereby conferring concavity upon the first term within the problem formulation. Hence, under the given conditions, we establish the concavity of $\text{Tr}(\mathbf{X} \tilde{\mathbf{C}} \mathbf{X}^\top)$, as stated. ■

In (55), the concave term $\text{Tr}(\mathbf{X} \tilde{\mathbf{C}} \mathbf{X}^\top)$ is linearized at the point $\mathbf{X} = \mathbf{X}_t$ through a first-order Taylor series expansion, similar to (39). This linearization allows us to derive an upperbound, from which we obtain

$$\begin{aligned} \tilde{f}(\mathbf{X} | \mathbf{X}_t) & \leq \min_{\mathbf{X} \succeq 0} \sum_{i=1}^N \|\mathbf{X}_t \tilde{\mathbf{b}}_i\| - \text{Tr}(\mathbf{X}_t \tilde{\mathbf{C}} \mathbf{X}_t^\top) + 2\text{Tr}(\mathbf{X}_t \tilde{\mathbf{C}} \mathbf{X}^\top) \\ & + \lambda_1 \text{Tr}(\mathbf{X}^\top \mathbf{X}) + \text{Tr}(\mathbf{X} (\mathbf{U}_b + \mathbf{U}_l)^\top \mathbf{R} (\mathbf{U}_b - \mathbf{U}_l)) \\ & - \log \det(\mathbf{X}). \end{aligned} \quad (56)$$

Therefore, we have the following surrogate function minimization problem:

$$\begin{aligned} \min_{\mathbf{X} \succeq 0} & \text{Tr}(\mathbf{X} (2\tilde{\mathbf{C}} \mathbf{X}_t^\top + (\mathbf{U}_b + \mathbf{U}_l)^\top \mathbf{R} (\mathbf{U}_b - \mathbf{U}_l))) \\ & + \lambda_1 \text{Tr}(\mathbf{X}^\top \mathbf{X}) - \log \det(\mathbf{X}). \end{aligned} \quad (57)$$

Let $\mathbf{D} = 2\tilde{\mathbf{C}} \mathbf{X}_t^\top + (\mathbf{U}_b + \mathbf{U}_l)^\top \mathbf{R}^{-1} (\mathbf{U}_b - \mathbf{U}_l)$ and $\bar{\mathbf{D}} = 1/2(\mathbf{D} + \mathbf{D}^\top)$, we have

$$\min_{\mathbf{X} \succeq 0} \text{Tr}(\bar{\mathbf{D}} \mathbf{X}) + \lambda_1 \text{Tr}(\mathbf{X}^\top \mathbf{X}) - \log \det(\mathbf{X}). \quad (58)$$

The solution to the previously mentioned problem can be obtained through the eigenvalue decomposition of matrix and the solution of scalar equations. In order to expedite the resolution of the problem (58), we employ the following lemma [29] given by

Lemma 3: Given any $N \times N$ real matrix \mathbf{E} and real symmetric matrix \mathbf{F} , where $\bar{\mathbf{E}} = 1/2(\mathbf{E} + \mathbf{E}^\top)$, then

$$\text{Tr}(\mathbf{EF}) \leq \sum_{i=1}^N \lambda_i(\bar{\mathbf{E}}) \lambda_i(\mathbf{F}), \quad (59)$$

where $\lambda_i(\bar{\mathbf{E}})$ and $\lambda_i(\mathbf{F})$ are the eigenvalues of $\bar{\mathbf{E}}$ and \mathbf{F} , respectively.

Let $\bar{\mathbf{D}} = \mathbf{V} \Sigma \mathbf{V}^\top$ represent the eigenvalue decomposition of $\bar{\mathbf{D}}$, where \mathbf{V} denotes the eigenvector matrix, and Σ contains the eigenvalues. Assuming the eigenvalue decomposition of the matrix \mathbf{X} can be written as $\mathbf{X} = \mathbf{Q} \Lambda \mathbf{Q}^\top$, where \mathbf{Q} is the eigenvector matrix, and Λ represents an unknown matrix. Consequently, $\text{Tr}(\bar{\mathbf{D}} \mathbf{X}) = \text{Tr}(\mathbf{V} \Sigma \mathbf{V}^\top \mathbf{Q} \Lambda \mathbf{Q}^\top)$ can be simplified by applying Lemma 3 as follows:

$$\text{Tr}(\bar{\mathbf{D}} \mathbf{X}) = \text{Tr}(\Sigma \Lambda) \quad (60)$$

with equality holding if and only if $\mathbf{V} = \mathbf{Q}$. Therefore, (58) can be expressed solely as a function of Λ . This can be written as:

$$\min_{\Lambda} \text{Tr}(\Sigma \Lambda) + \lambda_1 \text{Tr}(\Lambda^\top \Lambda) - \log \det(\Lambda). \quad (61)$$

It's noteworthy that (61) serves as an upper bound for the original problem stated in (57).

The problem (61) becomes:

$$\min_{\gamma_i > 0} \sum_{i=1}^N \sigma_i^o \gamma_i + \lambda_1 \gamma_i^2 - \log \prod_{i=1}^N \gamma_i. \quad (62)$$

where γ_i and σ_i^o represent the eigenvalues of matrixes \mathbf{X} and \mathbf{D} , respectively.

A generic problem can be expressed as follows, without the index i :

$$\min_{\gamma > 0} \sigma^o \gamma + \lambda_1 \gamma^2 - \log(\gamma). \quad (63)$$

The Karush-Kuhn-Tucker (KKT) condition for the problem (61) will be

$$\sigma^o + 2\lambda_1 \gamma - \frac{1}{\gamma} = 0, \quad (64)$$

which can also be written as:

$$\gamma \sigma^o + 2\lambda_1 \gamma^2 - 1 = 0. \quad (65)$$

By solving the KKT conditions, we obtain the optimal solution for γ , and this will be used as the next iteration step.

$$\gamma = \frac{-\sigma^o + \sqrt{(\sigma^o)^2 + 8\lambda_1}}{4\lambda_1}. \quad (66)$$

This expression simplifies to a quadratic equation, and its positive real root yields the optimal solution Λ^{opt} . The overall pseudocode of the proposed DIMM algorithm is given in Algorithm 1. Pseudocode of the proposed algorithm to update \mathbf{X} is given in Algorithm 2.

C. Analysis of Computational Complexity and Convergence

The analysis of computational complexity for the proposed algorithm is as follows. In each iteration of the proposed DIMM method, updating the primal variables for the two optimal designs requires calculating matrices \mathbf{H}_l and \mathbf{A} , resulting in a computational complexity of $O(N^2 n)$. Here, n represents the dimension of the state vector. Additionally, updating the dual variable for the D optimal designs involves calculations related to \mathbf{X} , $\tilde{\mathbf{C}}$, and $\lambda_{\max}(\tilde{\mathbf{C}})$, including $O(Nn^2)$

Algorithm 1 Pseudocode of the Proposed DIMM Algorithm

- 1: **Input:** \mathbf{R}^{-1} and $\epsilon = 10^{-3}$
- 2: **Output:** The value of \mathbf{U}^{opt} is derived upon reaching convergence in the loop.
- 3: Initialization: \mathbf{U}_0 and \mathbf{X}_0
- 4: **while** $\|\mathbf{U}_{l+1} - \mathbf{U}_l\|/\|\mathbf{U}_l\| \leq \epsilon$ **do**
- 5: Compute \mathbf{U}_l and $\tilde{\mathbf{C}}$
- 6: Update \mathbf{X} using Algorithm 2
- 7: Compute \mathbf{A} and then solve (48) to get \mathbf{U}_{l+1}
- 8: **end while**

Algorithm 2 Pseudocode of the Proposed Algorithm to Update \mathbf{X}

- 1: **Input:** $\epsilon = 10^{-3}$
- 2: **Output:** \mathbf{X}
- 3: **while** $\|\mathbf{X}_{t+1} - \mathbf{X}_t\|/\|\mathbf{X}_t\| \leq \epsilon$ **do**
- 4: Compute $\tilde{\mathbf{C}}$, $\lambda_{\max}(\tilde{\mathbf{C}})$ and $\tilde{\mathbf{D}}$
- 5: Compute the EVD $\tilde{\mathbf{D}} = \mathbf{V}\Sigma\mathbf{V}^\top$
- 6: Solve (66) to obtain $\mathbf{\Lambda}^{\text{opt}}$
- 7: $\mathbf{X}_{t+1} = \mathbf{V}\mathbf{\Lambda}^{\text{opt}}\mathbf{V}^\top$
- 8: **end while**

operations for matrix \mathbf{D} and an eigenvalue decomposition of \mathbf{D} , involving $O(n^3)$ flops within each inner loop iteration. The proposed algorithm's computational complexity for \mathbf{D} optimal designs converges to $O(N^2n)$, given that the number of measurements N usually exceeds the number of variables n . In the ADMM method mentioned in [30], the main computational burden lies in updating the variable \mathbf{u} to solve the semidefinite programming (SDP) problem, which is addressed using the interior-point method. According to [31], the average worst case computation complexity of SDP problem is of the order $O(N^{4.5})$. In 5G positioning scenarios, the number of measurements N is generally much greater than the number of states n , making the proposed method computationally less complex than the ADMM approach.

The iterative process involving MM updates applied to the dual variable \mathbf{X} within the DIMM algorithm ensures convergence towards the global optimal solution of the dual problem(51). The inherent convexity of the dual problem ensures that the attained stationary point is, simultaneously, the global minimizer of $f(\mathbf{X})$. Simultaneously, the iterative procedures governing MM updates for the primal variable \mathbf{U} in our proposed algorithm lead to convergence by the KKT condition for the problem (36).

V. SIMULATIONS

In this section, we delve into various numerical simulations involving optimal UAV placement and design parameters. The primary objective is to thoroughly evaluate the performance of the proposed DIMM method.

A. Optimal UAV Configuration and Minimum Achievable Variance for Multistatic 5G Localization

We initially examine the optimal configurations for TOA multistatic localization. These configurations involve one

transmitter and N available UAVs. The resultant optimal configuration dictates that half of the UAVs should possess an bearing angle of $\pi/3$, while the remaining half should hold an bearing angle of $-\pi/3$. It's important to note that the arrangement permutations of UAVs do not influence optimality, given the equal noise variances across different UAVs. The strategic placement of multiple UAVs along bearing lines with angles of $\pm\pi/3$ radians serves the purpose of minimizing the target estimate error covariance.

Fig. 2 depicts the behavior of the determinant of the FIM concerning variations in θ_2 and θ_3 , with $\theta_1 = \pi/3$. Fig. 2 illustrates the locations of maxima with a '+' sign for three distinct cases:

- When the standard deviations of all UAVs are equal $\sigma_1 = \sigma_2 = \sigma_3 = 0.1$, the maxima of the FIM determinant occur at $\{\theta_2^*, \theta_3^*\} = \{-\pi/3, -\pi/3\}, \{-\pi/3, \pi/3\}$, and $\{\pi/3, -\pi/3\}$.
- In the case of non-uniform UAV variances $\sigma_1 = 0.1$, $\sigma_2 = \sigma_3 = 0.05$, the maxima of the FIM determinant occur at $\{\theta_2^*, \theta_3^*\} = \{\pi/3, -\pi/3\}$ and $\{-\pi/3, \pi/3\}$.
- For another set of non-uniform UAV variances $\sigma_1 = 0.1$, $\sigma_2 = 0.2$, and $\sigma_3 = 0.3$, the maxima of the FIM determinant occur at $\{\theta_2^*, \theta_3^*\} = \{-\pi/3, -\pi/3\}$.

These results are highly significant as they reveal the optimal configurations of θ_2 and θ_3 that yield maximum values of the FIM determinant for different UAV variance scenarios. Fig. 2 provides crucial insights into how the geometric arrangement of UAVs can affect the localization accuracy of the target.

Fig. 3 depicts the relationship between σ and the carrier-to-noise ratio C/N_0 across various 5G system bandwidths, taking into account the potential range of C/N_0 in the context of a 5G scenario. The C/N_0 limits are defined for two primary network designs characterized by high and low intersite distances (ISD), denoted as ρ with values of 116 m and 5 m, respectively. In the first scenario, assuming maximum path losses, the ultra-dense network scenario path loss model yields a path loss of approximately 132.59 dB for $d = 120 : \text{m}$ at $f = 30\text{GHz}$. Utilizing maximum power $P_{\max} = 43 : \text{dBm}$ and shadow fading SF = $2\sigma_{\text{SF}}$, the corresponding C/N_0 limit is 72.91 dB-Hz. This limit restricts achieving a target accuracy of 30 cm to signal bandwidths exceeding 50 MHz. In the second scenario, considering minimum path losses, the ultra-dense network scenario path loss model results in a path loss of approximately 83.75 dB for $d = 5 : \text{m}$ at $f = 30 : \text{GHz}$. Consequently, with $P_{\max} = 43 : \text{dBm}$ and SF = $2\sigma_{\text{SF}}$, the C/N_0 limit is 121.15 dB-Hz, enabling the achievement of the target accuracy with any signal bandwidth. Fig. 3 illustrates these two C/N_0 limits.

B. Initialization and Preliminary Results

In this subsection, we apply the proposed algorithm to ascertain the optimal UAV placement around the target, with the aim of enhancing localization accuracy. For the purpose of simplicity, we assume that the target is approximately situated at the origin, denoted as $\mathbf{p} = [0, 0]^\top$.

For this analysis, we consider three UAVs to be strategically positioned on a circle with radius r . Initially, the UAVs are

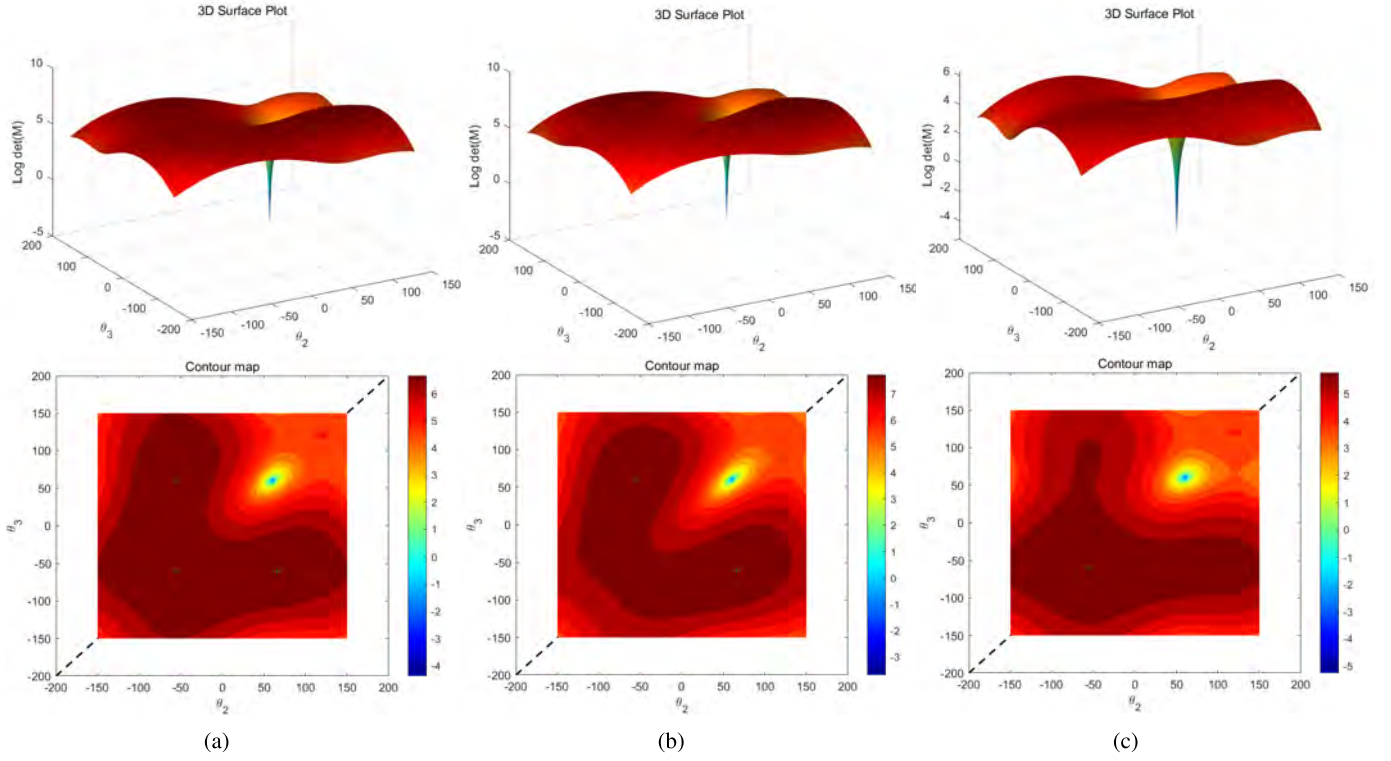


Fig. 2. The $\det(\mathbf{M})$ varies as a function of θ_2 and θ_3 with $\theta_1 = 60^\circ$.

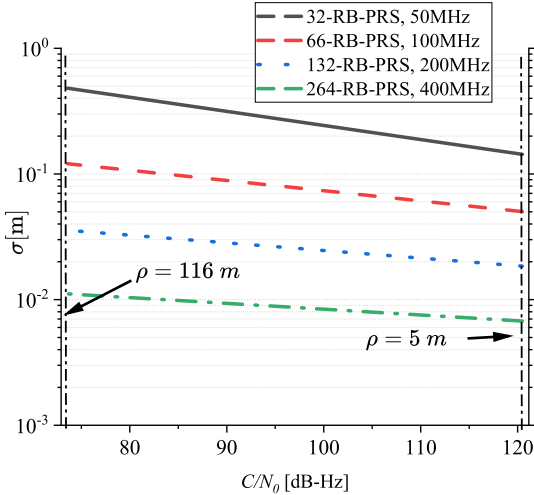


Fig. 3. Plot of σ as a function of the carrier-to-noise ratio C/N_0 by using different 5G system bandwidths, and considering the possible range of C/N_0 in the 5G scenario.

randomly distributed along the circle's circumference. In the proposed algorithm, the primal variable \mathbf{U} is initialized with the known UAV positions, while the variable \mathbf{X} is set to $\mathbf{X}_0 = (\mathbf{H}^T \mathbf{R}^{-1} \mathbf{H})^{-1}$. This value represents the solution to the Fenchel dual problem. The root mean square error is taken as the performance measure which is computed as:

$$\text{RMSE} = \sqrt{\frac{1}{N} \sum_{i=1}^N \|\mathbf{p} - \hat{\mathbf{p}}\|^2}, \quad (67)$$

where $\hat{\mathbf{p}}$ is the estimated target position.

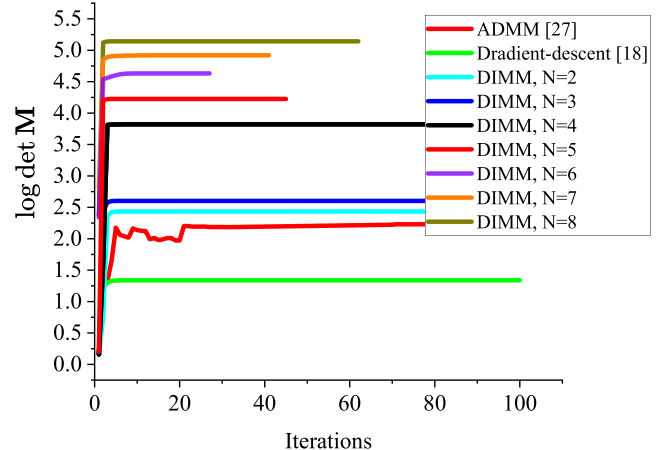


Fig. 4. Performance comparsion of various methods for multistatic 5G localization.

The measurements are affected by correlated noise characterized by zero mean and positive definite covariance matrices. For analysis of the multistatic localization, we adopt the Maximum Likelihood (ML) to estimate the target position and evaluate the effect on the optimal geometry. TABLE I describes the positioning performance of the two geometric placement, where initial geometry and optimal geometry (after processing by DIMM algorithm) formed by UAVs and the target in presence of correlated measurement noise. The initialization method utilizing uniform placement facilitates a comparison, in terms of the design objective, between the uniform UAV geometry and the optimal UAV arrangement

TABLE I
POSITIONING PERFORMANCE

Geometry (2D)	$\log \det \mathbf{M}$	RMSE (ML) [m]
Optimal	2.60	1.34
Initial	0.69	5.26

derived from the proposed algorithm. The optimal UAV configuration achieved through the proposed algorithm, employing D optimal designs, demonstrates a substantial enhancement of 40% to 70% compared to the uniform placement strategy. This underscores the potential for enhancing localization accuracy through the UAV-target geometry derived from the proposed algorithm. The multistatic positioning performance improves noticeably when the optimal receiver configuration is achieved.

C. Performance in the Presence of Uncorrelated Noise Measurements for Multistatic 5G Localization

In the following analysis, we assess the performance of the DIMM algorithm under independent noise conditions. To achieve this, we focus on UAV placement with a fixed distance from the target, and measurements are influenced by diagonal noise covariance matrices represented as $\mathbf{R} = \text{diag}(\sigma_1^2, \dots, \sigma_N^2)$.

The following baselines are implemented for the performance comparison. For the ADMM-based method, please refer to [30]. The additional contents present an iterative gradient descent method [18] designed to handle real-time processing of measurements as they are acquired, enabling the determination of an optimal trajectory for each UAV. The online nature of these computations offers the added advantage of adaptive optimization, allowing for the adjustment of UAV trajectories in response to changes in the geolocation scenario:

$$\mathbf{s}(n+1) = \mathbf{s}(n) + \mathbf{Q}(n) \frac{\partial J_T(\mathbf{s}(n))}{\partial \mathbf{s}(n)}, \quad (68)$$

where $\mathbf{s}(n) = [\mathbf{r}_1, \dots, \mathbf{r}_N]^\top$ is a vector stacking the positions of all UAVs at the n th iteration, $\mathbf{Q}(n)$ is a time-varying step-size matrix which ensures each UAV moves along the direction guided by the gradient for a uniform distance between successive iterations, and $J_T(\mathbf{s}(n)) = \det(\mathbf{M})$ is the cost function (the determinant of FIM) to be maximized. The first-order finite difference approximation is used to compute the gradient of $J_T(\mathbf{s}(n))$, where the constant in (28) of [32] is set to $\Delta = 0.01$ m. Since $\det(\mathbf{M})$ cannot be computed as the true target location is unknown, it is approximated using the target position estimate obtained from the iterative linearized least squares estimator for multistatic TOA localization. In an attempt to realize the fastest convergence to the maximum of $J_T(\mathbf{s}(n))$, the gradient of $J_T(\mathbf{s}(n))$ is normalized by the step-size matrix $\mathbf{Q}(n)$. The normalization aims to move each receiver along the direction set by the gradient at maximum speed v_{max} , thus covering a uniform distance of $\mu = v_{max}\Delta t$ for each receiver where Δt is the time interval between successive UAV location updates in (25) of [32]. The resulting

step-size matrix is

$$\mathbf{Q}(n) = \mu \begin{bmatrix} \mu_1 \mathbf{I}_2 & & \mathbf{0} \\ & \ddots & \\ \mathbf{0} & & \mu_N \mathbf{I}_2 \end{bmatrix}, \quad \mu_i = \frac{1}{\|\partial J_T(\mathbf{s}(n))/\partial \mathbf{r}_i(n)\|_2}, \quad (69)$$

where \mathbf{I}_2 denotes the 2×2 identity matrix.

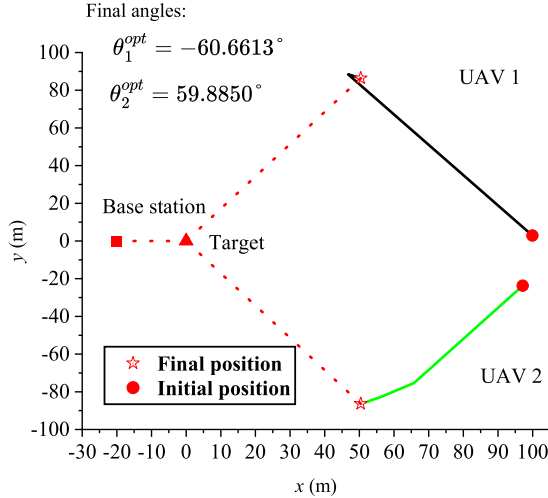
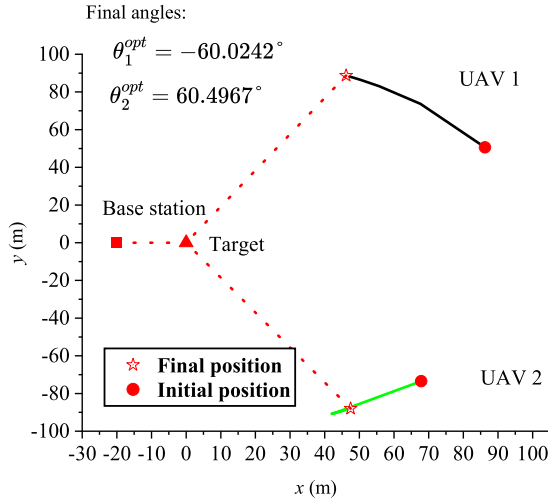
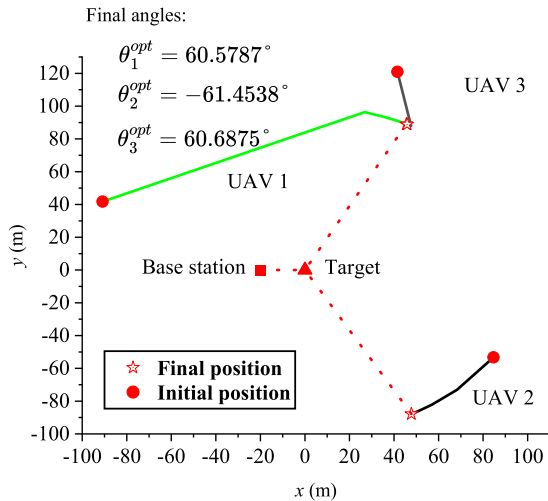
In Fig. 4, we compare the performance of DIMM, gradient-descent [18], and ADMM [30] algorithms, where $N = 3$. Regardless of the number of UAVs ($N \geq 2$), it can be seen that the performance of the proposed DIMM algorithm is better than gradient-descent and ADMM methods. The DIMM method and gradient-descent method have faster convergence compared with ADMM. As the number of UAVs increases, the value of $\log \det(\mathbf{M})$ function also rises. This demonstrates that increasing the number of UAVs improves 5G positioning performance in multistatic scenarios. Furthermore, the results confirm that the proposed method maintains scalability and efficiency even for higher values of N . To achieve maximum localization accuracy, it is essential to position the UAVs in their respective optimal configurations. These optimal configurations can be determined using the proposed DIMM algorithm.

We presume that the distances from the UAVs to the target are evenly spaced, represented as $\|\mathbf{p} - \mathbf{r}_i\| = r_i$. For the subsequent simulations, we set $r_i = r = 100$ m, and position the transmitter at coordinates (-20 m, 0 m). Figs. 5-8 illustrate the simulated optimal trajectories of the UAVs, alongside the different measurement variances for the cases of $N = 2$ and 3. This paper primarily centers on achieving optimal angular separation. To achieve this goal without assuming a fixed radius, UAVs not only move to positions that offer optimal angular separation but also move toward the target. This movement is driven by the reduction in measurement error variance effected by SNR and path loss as transmitters and UAVs approach the target.

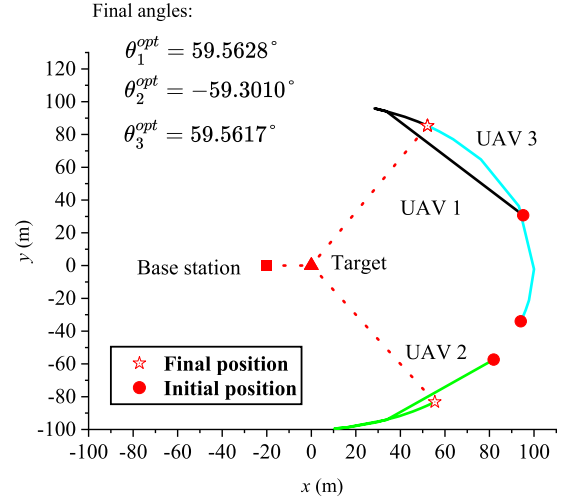
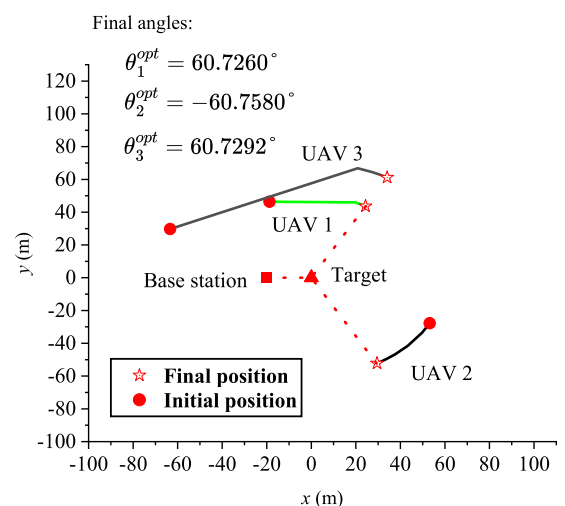
For the analysis of the optimal placement for nonuniform r_i , we have considered configuration problem of placing 3 UAVs as depicted in Fig. 9 and Fig. 10. In this scenario, the noise variances remain consistent with the previously mentioned values. However, the UAV-target ranges are altered to $r_1 = 50$ m, $r_2 = 60$ m, and $r_3 = 70$ m. It is observed that the final angular geometries obtained by the UAVs will not be influenced by nonuniform r_i .

D. Mean Square Error (MSE) Analysis

In this section, we investigate the enhancement in target localization accuracy facilitated by the UAV positions obtained through our proposed methodology. We will juxtapose the MSE of the target location, derived using the optimal UAV placement from our approach, against the MSE of estimates acquired through uniform and random UAV arrangements. The target location estimate is derived using the ML technique. For the simulation, we consider the following configuration: The target is assumed to be positioned at $[0, 0]^\top$ m, while the UAVs are distributed along the circumference of a unit

Fig. 5. The optimal trajectories for $N = 2$ with $\sigma_1 = \sigma_2 = 1$.Fig. 6. The optimal trajectories for $N = 2$ with $\sigma_1 = 1, \sigma_2 = 2$.Fig. 7. The optimal trajectories for $N = 3$ with $\sigma_1 = \sigma_2 = \sigma_3 = 1$.

radius circle. The uniform and random UAV geometries are established by positioning the UAVs uniformly and randomly around the circumference, whereas the optimal

Fig. 8. The optimal trajectories for $N = 3$ with $\sigma_1 = 1, \sigma_2 = 2, \sigma_3 = 3$.Fig. 9. The optimal trajectories for $N = 3$, considering varying noise variances, are examined at equal variances ($\sigma_1 = \sigma_2 = \sigma_3 = 1$), different distances ($r_1 = 50$ m, $r_2 = 60$ m, $r_3 = 70$ m) from UAV i to the target.TABLE II
COMPARISON OF THE ML PERFORMANCE FOR DIFFERENT PLACEMENT

Number of UAVs	Placement	MSE (in sq. meters)
$N = 3$	Random	1.25
	Uniform	1.22
	Optimal	0.89
$N = 4$	Random	0.95
	Uniform	0.88
	Optimal	0.69
$N = 5$	Random	0.82
	Uniform	0.71
	Optimal	0.55

geometry is determined using the DIMM algorithm. The MSE values of the MLE, obtained via 1000 Monte Carlo simulations, are detailed in Table II. These outcomes reveal that the MSE of estimates achieved through optimal placement via our proposed approach are notably smaller than those from other placement strategies.

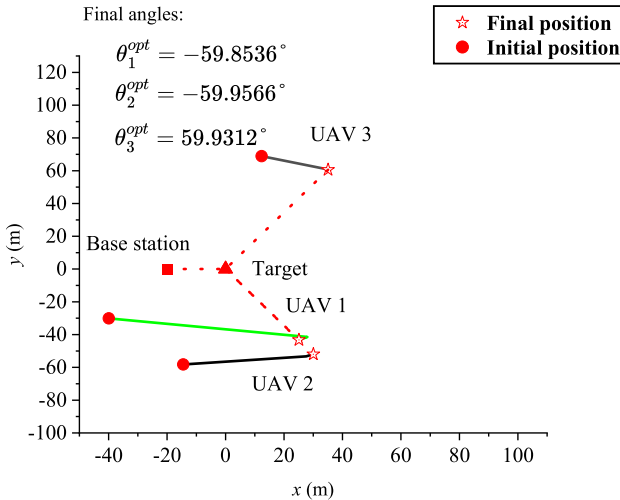


Fig. 10. The optimal trajectories for $N = 3$, considering varying noise variances, are examined at different variances ($\sigma_1 = 1, \sigma_2 = 2, \sigma_3 = 3$), different distances ($r_1 = 50$ m, $r_2 = 60$ m, $r_3 = 70$ m) from UAV i to the target.

TABLE III

COMPARATIVE ANALYSIS OF MAXIMUM LIKELIHOOD ESTIMATION PERFORMANCE FOR UAV PLACEMENT IN TARGET LOCALIZATION WITH MISMATCH

Number of UAVs	Target Position	MSE (in sq. meters)
$N = 3$	True position	1.21
	Position with Error 1	1.36
	Position with Error 2	1.30
$N = 4$	True position	0.42
	Position with Error 1	0.53
	Position with Error 2	0.48
$N = 5$	True position	0.35
	Position with Error 1	0.44
	Position with Error 2	0.47

The optimal placement of UAVs is devised based on an initial estimation of the target's position. However, this preliminary estimation may be inherently imprecise, deviating significantly from the true target location. Therefore, in the following, we investigate the effectiveness of the proposed algorithm when confronted with discrepancies between the assumed and true target positions used during the design phase. We introduce variations in the target position employed in the design, deliberately setting it slightly apart from the true position. Subsequently, we compare the MSE of the location estimates obtained by the proposed algorithm under these conditions with two scenarios of target location mismatch. Specifically, we examine the placement of UAVs along the circumference of a unit circle with the target positioned at its center. The results of the MSE analysis for varying numbers of UAVs are presented in Table III. Remarkably, the MSE values for the cases involving target position mismatches exhibit only marginal increases compared to the scenario assuming the true target position during design. This finding underscores the robustness of the design against discrepancies in the input parameters, affirming the algorithm's reliability under diverse conditions of target localization.

VI. CONCLUSION

In this study, the domain of multistatic TOA localization has been subject to notable attention, primarily due to the inherent performance benefits it offers. The interplay between the relative geometry of UAVs and targets plays a pivotal role in shaping the outcome of target localization efforts, significantly influencing the overall performance.

This study presents a novel approach to advancing UAV localization through the refinement of localization models and the establishment of novel optimization criteria. The conventional derivation of the CRLB for TOA-based multistatic localization undergoes a transformative redefinition. By embracing unit norm vectors in lieu of traditional trigonometric parameterizations, this innovative approach simplifies design and algorithm development. Notably, it provides a streamlined means of accommodating the nuanced variations in CRLB matrix expressions linked to TOA measurement models. Expanding upon this foundation, we formulate optimization objectives rooted in the principles of D-optimal criteria, all anchored in the foundation of the CRLB. A noteworthy outcome is the development of a unique DIMM algorithm. This approach, unlike state-of-the-art MM techniques, orchestrates updates for both primal and dual variables, harnessing the synergy between them. Through the utilization of a saddle-point problem framework and inventive upper-bound constraints, the DIMM algorithm exhibits its effectiveness. A comprehensive computational complexity analysis corroborates the practical feasibility of our proposed methodology. Extensive simulations, conducted under diverse noise variances and across a spectrum of UAV-target distances, validate the robustness and effectiveness of our approach.

Theoretically, the method proposed in this paper is promising for multi-target localization scenarios. However, two important challenges need to be identified here. The first challenge lies in constructing an appropriate optimization function, which can vary based on the specific objectives. For example, the function might be formulated to minimize localization uncertainty for a single, high-priority target, or alternatively, to ensure uniform accuracy across multiple targets. In some cases, certain targets may be given higher priority than others, depending on the desired outcome. Once the optimization objective is defined, the next challenge is to determine the feasibility of solving the resulting problem. This includes assessing whether a closed-form solution exists or if alternative numerical methods are necessary to achieve convergence.

REFERENCES

- [1] Y. Zhang, R. Wang, and Z. Xing, "A robust evolutionary particle filter technique for integrated navigation in urban environments via GNSS and 5G signals," *IEEE Trans. Ind. Informat.*, vol. 20, no. 4, pp. 6866–6878, Apr. 2024.
- [2] Y. Zhang, R. Wang, and Z. Xing, "Collaborative navigation in urban environments via GNSS and 5G signals," in *Proc. ICC - IEEE Int. Conf. Commun.*, May 2023, pp. 6275–6280.
- [3] Y. Li et al., "Cooperative elliptic positioning through single UAV during GNSS outages," *IEEE Trans. Wireless Commun.*, vol. 23, no. 10, pp. 12749–12764, Oct. 2024.
- [4] K. Li, R. C. Voicu, S. S. Kanhere, W. Ni, and E. Tovar, "Energy efficient legitimate wireless surveillance of UAV communications," *IEEE Trans. Veh. Technol.*, vol. 68, no. 3, pp. 2283–2293, Mar. 2019.

- [5] K. Li, W. Ni, X. Wang, R. P. Liu, S. S. Kanhere, and S. Jha, "Energy-efficient cooperative relaying for unmanned aerial vehicles," *IEEE Trans. Mobile Comput.*, vol. 15, no. 6, pp. 1377–1386, Jun. 2016.
- [6] X.-H. Lin et al., "Joint optimization of resource allocation and flight trajectory for UAV-IoT underwater detecting systems," *IEEE Trans. Veh. Technol.*, vol. 72, no. 12, pp. 16482–16498, Dec. 2023.
- [7] D. Malioutov, M. Cetin, and A. S. Willsky, "A sparse signal reconstruction perspective for source localization with sensor arrays," *IEEE Trans. Signal Process.*, vol. 53, no. 8, pp. 3010–3022, Aug. 2005.
- [8] Y. Kang, Q. Wang, J. Wang, and R. Chen, "A high-accuracy TOA-based localization method without time synchronization in a three-dimensional space," *IEEE Trans. Ind. Informat.*, vol. 15, no. 1, pp. 173–182, Jan. 2019.
- [9] M. Beard, S. Reuter, K. Granström, B.-T. Vo, B.-N. Vo, and A. Scheel, "Multiple extended target tracking with labeled random finite sets," *IEEE Trans. Signal Process.*, vol. 64, no. 7, pp. 1638–1653, Apr. 2016.
- [10] Y. Zhang, X. Tan, and C. Zhao, "UWB/INS integrated pedestrian positioning for robust indoor environments," *IEEE Sensors J.*, vol. 20, no. 23, pp. 14401–14409, Dec. 2020.
- [11] A. Fotouhi et al., "Survey on UAV cellular communications: Practical aspects, standardization advancements, regulation, and security challenges," *IEEE Commun. Surveys Tuts.*, vol. 21, no. 4, pp. 3417–3442, 2019.
- [12] A. N. Bishop, B. Fidan, B. D. O. Anderson, K. Dogançay, and P. N. Pathirana, "Optimality analysis of sensor-target localization geometries," *Automatica*, vol. 46, no. 3, pp. 479–492, Mar. 2010.
- [13] S. Martínez and F. Bullo, "Optimal sensor placement and motion coordination for target tracking," *Automatica*, vol. 42, no. 4, pp. 661–668, 2006.
- [14] C. Yang, L. Kaplan, E. Blasch, and M. Bakich, "Optimal placement of heterogeneous sensors for targets with Gaussian priors," *IEEE Trans. Aerosp. Electron. Syst.*, vol. 49, no. 3, pp. 1637–1653, Jul. 2013.
- [15] F. Penna, M. A. Caceres, and H. Wymeersch, "Cramér-Rao bound for hybrid GNSS-terrestrial cooperative positioning," *IEEE Commun. Lett.*, vol. 14, no. 11, pp. 1005–1007, Nov. 2010.
- [16] Z. M. Kassas, A. Arapostathis, and T. E. Humphreys, "Greedy motion planning for simultaneous signal landscape mapping and receiver localization," *IEEE J. Sel. Topics Signal Process.*, vol. 9, no. 2, pp. 247–258, Mar. 2015.
- [17] R. Amiri, F. Behnia, and M. A. M. Sadr, "Exact solution for elliptic localization in distributed MIMO radar systems," *IEEE Trans. Veh. Technol.*, vol. 67, no. 2, pp. 1075–1086, Feb. 2018.
- [18] N. H. Nguyen and K. Dogancay, "Optimal geometry analysis for multistatic TOA localization," *IEEE Trans. Signal Process.*, vol. 64, no. 16, pp. 4180–4193, Aug. 2016.
- [19] L. Rui and K. C. Ho, "Elliptic localization: Performance study and optimum receiver placement," *IEEE Trans. Signal Process.*, vol. 62, no. 18, pp. 4673–4688, Sep. 2014.
- [20] S. Zhao, B. M. Chen, and T. H. Lee, "Optimal sensor placement for target localisation and tracking in 2D and 3D," *Int. J. Control.*, vol. 86, no. 10, pp. 1687–1704, Oct. 2013.
- [21] K. Dogancay, "UAV path planning for passive emitter localization," *IEEE Trans. Aerosp. Electron. Syst.*, vol. 48, no. 2, pp. 1150–1166, Apr. 2012.
- [22] Y. Oshman and P. Davidson, "Optimization of observer trajectories for bearings-only target localization," *IEEE Trans. Aerosp. Electron. Syst.*, vol. 35, no. 3, pp. 892–902, Jul. 1999.
- [23] D. Ucinski, *Optimal Measurement Methods for Distributed Parameter System Identification*. Boca Raton, FL, USA: CRC Press, 2004.
- [24] K. Shamaei and Z. M. Kassas, "Receiver design and time of arrival estimation for opportunistic localization with 5G signals," *IEEE Trans. Wireless Commun.*, vol. 20, no. 7, pp. 4716–4731, Jul. 2021.
- [25] Y. Zhang, R. Wang, E. Liu, B. Li, and H. Ge, "Asynchronous time-of-arrival-based 5G localization: Methods and optimal geometry analysis," *IEEE Internet Things J.*, vol. 11, no. 20, pp. 33994–34008, Oct. 2024.
- [26] H. Ni et al., "Path loss and shadowing for UAV-to-ground UWB channels incorporating the effects of built-up areas and airframe," *IEEE Trans. Intell. Transp. Syst.*, vol. 25, no. 11, pp. 17066–17077, Nov. 2024.
- [27] J. A. Del Peral-Rosado, J. A. Lopez-Salcedo, S. Kim, and G. Seco-Granados, "Feasibility study of 5G-based localization for assisted driving," in *Proc. Int. Conf. Localization GNSS (ICL-GNSS)*, Jun. 2016, pp. 1–6.
- [28] G. Fatima, Z. Li, A. Arora, and P. Babu, "PDMM: A novel primal-dual majorization-minimization algorithm for Poisson phase-retrieval problem," *IEEE Trans. Signal Process.*, vol. 70, pp. 1241–1255, 2022.
- [29] B.-Y. Wang and F. Zhang, "Trace and eigenvalue inequalities for ordinary and Hadamard products of positive semidefinite Hermitian matrices," *SIAM J. Matrix Anal. Appl.*, vol. 16, no. 4, pp. 1173–1183, Oct. 1995.
- [30] E. Tzoreff and A. J. Weiss, "Path design for best emitter location using two mobile sensors," *IEEE Trans. Signal Process.*, vol. 65, no. 19, pp. 5249–5261, Oct. 2017.
- [31] Z.-Q. Luo, W.-K. Ma, A. M.-C. So, Y. Ye, and S. Zhang, "Semidefinite relaxation of quadratic optimization problems," *IEEE Signal Process. Mag.*, vol. 27, no. 3, pp. 20–34, May 2010.
- [32] K. Doganay, "Online optimization of receiver trajectories for scan-based emitter localization," *IEEE Trans. Aerosp. Electron. Syst.*, vol. 43, no. 3, pp. 1117–1125, Jul. 2007.



Yuan Zhang (Graduate Student Member, IEEE) received the B.S. degree in surveying and mapping engineering from Shandong University of Science and Technology, Qingdao, China, in 2017, the M.S. degree in geodesy and surveying engineering from Jiangsu Normal University, Xuzhou, China, in 2020, and the Ph.D. degree in information and communication engineering from the College of Electronics and Information Engineering, Tongji University, Shanghai, China, in 2024.

He is currently a Lecturer with the School of Mechanical and Automotive Engineering, Anhui University of Engineering, Wuhu, China. His research interests include GNSS/5G and multisensor integration for future accurate positioning. Additionally, he focuses on optimal sensor placement, estimation, and optimization algorithms. He serves as a reviewer for several IEEE journals, including IEEE TRANSACTIONS ON WIRELESS COMMUNICATIONS, IEEE TRANSACTIONS ON INDUSTRIAL INFORMATICS, IEEE TRANSACTIONS ON INDUSTRIAL ELECTRONICS, IEEE INTERNET OF THINGS JOURNAL, IEEE SIGNAL PROCESSING LETTERS, and IEEE SENSORS JOURNAL.



Rui Wang (Senior Member, IEEE) received the Ph.D. degree from Shanghai Jiao Tong University, China, in 2013.

From August 2012 to February 2013, he was a Visiting Ph.D. Student with the Department of Electrical Engineering, University of California at Riverside. From October 2013 to October of 2014, he was with the Institute of Network Coding, The Chinese University of Hong Kong, as a Post-Doctoral Research Associate. From October 2014 to December 2016, he was with the College of Electronics and Information Engineering, Tongji University, as an Assistant Professor, where he is currently a Full Professor. He has published over 60 articles. His research interests include wireless communications, artificial intelligence, and wireless positioning. He received Shanghai Excellent Doctor Degree Dissertation Award in 2015 and the ACM Shanghai Rising Star Nomination Award in 2016. He is currently an Associate Editor of IEEE ACCESS and an Editor of the IEEE WIRELESS COMMUNICATIONS LETTERS.



Erwu Liu (Senior Member, IEEE) received the Ph.D. degree from the Huazhong University of Science and Technology, China, in 2001.

He has been a Professor with Tongji University since 2011. Previously, he was with Alcatel-Lucent, from 2001 to 2007, and Imperial College London, from 2007 to 2011. He currently leads Shanghai Engineering Research Center for Blockchain Applications and Services. He studies localization, blockchain, AI, and the Internet of Things, with more than 120 articles published and more than 70 patents granted/pending. He won the Microsoft Indoor Localization Competition (IPSN) in 2016 and 2018 and developed the well-known indoor navigation system for China International Import Expo. He is the Community Development Co-Chair of the IEEE Blockchain Technical Community and leads the local group development of the IEEE BCTC in Asia/China. He is an IET Fellow, the Founding Editor-in-Chief of *IET Blockchain*, and the Founding Chair of the IEEE Global Blockchain Conference.